Available online at www.sciencedirect.com

ScienceDirect

International Journal of Solids and Structures 44 (2007) 1643–1656

INTERNATIONAL JOURNAL OF SOLIDS and STRUCTURES

www.elsevier.com/locate/ijsolstr

Mixed numerical–experimental technique for orthotropic parameter identification using biaxial tensile tests on cruciform specimens

David Lecompte [a,*], Arwen Smits [b], Hugo Sol [b], John Vantomme [a], Danny Van Hemelrijck [b]

[a] *Royal Military Academy, Department of Civil and Materials Engineering, Av. De la Renaissance 30, 1000 Brussels, Belgium*
[b] *Vrije Universiteit Brussel, Mechanics of Materials and Constructions, Pleinlaan 2, 1050 Brussels, Belgium*

Received 13 February 2006; received in revised form 22 May 2006
Available online 21 July 2006

Abstract

This paper presents a mixed numerical–experimental method for the identification of the four in-plane orthotropic engineering constants of composite plate materials. A biaxial tensile test is performed on a cruciform test specimen. The heterogeneous displacement field is observed by a CCD camera and measured by a digital image correlation (DIC) technique. The measured displacement field and the subsequently computed strain field are compared with a finite element simulation of the same experiment. The four independent engineering constants are unknown parameters in the finite element model. Starting from an initial value, these parameters are updated till the computed strain field matches the experimental strain field. Two specimen geometries are used: one with a centered hole to increase the strain heterogeneity and one without a hole. It is found that the non-perforated specimen yields the most accurate results.

Keywords: Parameter identification; Biaxial testing; Digital image correlation

1. Introduction

Standard testing to obtain material parameters requires test samples with a well-defined standardised geometry. They commonly generate a uniaxial stress field that allows the identification of one or sometimes two material properties (Whitney et al., 1984; ASTM, 2000, 2001). For orthotropic material properties, different tests are needed to identify all the mechanical properties of the material. Actual structural components manufactured in factory or used in engineering (Meuwissen, 1998) are submitted to complex stress fields and show

* Corresponding author. Tel.: +32 2737 6413; fax: +32 2737 6412.
E-mail address: david.lecompte@rma.ac.be (D. Lecompte).

0020-7683/$ - see front matter
doi:10.1016/j.ijsolstr.2006.06.050

sometimes other material properties than those obtained by standard testing. In those cases, mixed numerical–experimental methods also called inverse methods for material parameter identification can improve the results. Mixed numerical–experimental methods are based on a finite element model of a complex test geometry. The technique proposed in this paper combines static loading experiments, optimisation techniques, full-field measurement techniques and a numerical finite element model.

The advantage of this inverse method is that non-standardised specimen geometries as well as detailed boundary conditions and complex material models can be taken into account. From an experimental point of view, the progress made during the last decade in the domain of optical full-field displacement techniques now allows the experimental identification of complex strain fields.

The aim of the mixed numerical–experimental method is to determine the different parameters in a single experimental set-up, allowing for the stresses and strains to exhibit heterogeneous patterns. In the past several attempts have been made to identify elastic parameters based on inverse modelling of different experimental set-ups. Some use uniaxial tensile tests on a perforated beam-like specimen (Molomard et al., 2005), others have used a transversely loaded rectangular plate (Wang and Kam, 2000), a circular disk under diametrical compression (Wang et al., 2005), a T-shaped specimen under tensile loading (Grédiac et al., 1999) or the displacement information around a hole in a biaxially loaded plate (Cárdenas-García et al., 2005).

The use of an inverse method is not limited to a single type of material. It has been used on materials like ceramics (Furgiuele et al., 1997), composite materials (Genovese et al., 2004), metallic materials (Meuwissen et al., 1998), micro-electronic mechanical systems (MEMS) (Amiot et al., 2005) and wood (Le Magorou et al., 2002). Different optical full-field techniques can be used for the measurement of the surface displacements. Examples in which electronic speckle pattern interferometry (Bruno and Poggialini, 2005), mark tracking (Szostkiewicz et al., 1997), geometric or interferometric Moiré (Cárdenas-García, 2000) or laser holographic interferometry (Zhu, 1996) are used, can be found in literature. In some cases the authors use the boundary element method (BEM) (Huang et al., 2004) or the virtual fields method (Grédiac et al., 2002) instead of the finite element method, but the overall principle remains identical.

The use of full-field measurement methods for the characterisation of composite materials is a topic which has been and which still is intensively studied by different authors. An interesting article containing 136 references related to this field has been published by Grédiac (Grédiac, 2004). In the present paper, a method is proposed for the identification of the four independent elastic in-plane engineering constants E_x, E_y, G_{xy} and v_{xy} of an orthotropic composite material based on surface measurements of a cruciform specimen subjected to biaxial loading. A biaxial tensile test is performed on a perforated cruciform specimen made out of glass fibre reinforced epoxy. As the material is supposed to behave homogeneously only one set of material parameters is determined. The responses of the system, i.e., the surface displacements are measured with digital image correlation. Strains are subsequently calculated, based on the measured displacement field. A finite element model of the perforated specimen serves as numerical counterpart for the experimental set-up. The difference between the experimental and numerical strains (ε_x, ε_y and γ_{xy}) is minimised in a least squares sense by updating the values of the four independent elastic moduli. The sensitivities used to obtain the parameter updates are determined analytically, using the stress values calculated during the previously converged step. This choice allows a convergence rate that is three times faster than a routine based on finite difference sensitivities. The optimisation routine uses a Newton–Raphson algorithm.

2. Experimental set-up

2.1. Biaxial testing

Different experimental techniques and specimens have been used to produce biaxial stress states. These techniques may be mainly classified into two categories (Zouani et al., 1996): (i) tests using a single loading system and (ii) tests using two or more independent loading systems. In the first category the biaxial stress ratio depends on the specimen geometry – their main disadvantage, – whereas in the second category it is specified by the applied load magnitude. Examples of the first category are bending tests on cantilever beams, anticlastic bending of rhomboidal shaped plates and bulge tests. Examples of the second category are thin-walled tubes subjected to a combination of tension/compression with torsion or internal/external pressure (Lefebvre

et al., 2000; Ellyn and Wolodko, 1995), and cruciform specimens under biaxial loading (Dawicke and Pollock, 2000). The most direct way to create biaxial stress states consists of applying in-plane loads along two perpendicular arms of cruciform specimens. The use of hydraulic actuators represents a very versatile technique for the application of the loads. The main difference between the existing techniques is the use of one or two actuators per loading direction. One actuator per loading direction (Chaudonneret et al., 1997) will cause movements of the centre of the specimen causing a side bending of the specimen. This results in undesirable non-symmetric strains. Systems with four actuators (Makinde et al., 1992; Shiratori and Ikegami, 1967; Yu et al., 2002) with a close-loop servo control using the measured loads as feedback system, allow the centre of the specimen standing still.

The plane biaxial test device using cruciform specimens developed at the Free University of Brussels has four independent servo-hydraulic actuators with an appropriate control unit to keep the centre of the specimen explicitly still. The device (Fig. 1) has a capacity of 100 kN in both perpendicular directions, but is restricted to tensile loads. As no cylinders with hydrostatic bearing were used, failure or slip in one arm of the specimen will result in sudden radial forces which could seriously damage the servo-hydraulic cylinders and the load cells. To prevent this, hinges were used to connect the specimen to the load cells and the servo-hydraulic cylinders to the test frame. Using four hinges for each loading direction results in an unstable situation in compression and consequently only tension loads can be performed.

In an ideal situation no displacement of the centre point of the specimen should be observed (Fig. 2(a)). Even when using four actuators, a small displacement might occur in a real situation and an imbalance arises in the forces (Fig. 2(b)). Due to a displacement in the y-direction for instance, a component F_y is added and the absolute value of the force $|P|$ is no longer equal to the absolute value of the force $|P'|$. However, as four load cells are used, it is possible to quantify this small load difference and to use this as a control signal.

The biaxial equipment used in the present study seems a little excessive for the identification of the elastic constants of orthotropic plate material. However, this machine is available in our lab and is also used for biaxial fatigue testing and the identification of hardening and yield surface parameters for metallic materials. Other devices, creating a biaxial loading state in a cruciform specimen and which can be mounted on a uniaxial tensile machine exist and could be considered as well (Ferron and Makinde, 1988).

2.2. Cruciform specimen

Traditional biaxial tests on cruciform specimens require at least the following conditions: (i) maximisation of the region of uniform biaxial strain and (ii) minimisation of the shear strains in the biaxially loaded test zone (Mayes et al., 2002). These conditions are required if strains are measured at the centre of the specimen with a strain gage or mechanical extensometer since one average strain value is obtained over their length. Since in this paper a full field method is used for the strain determination, non-uniformities and occurring

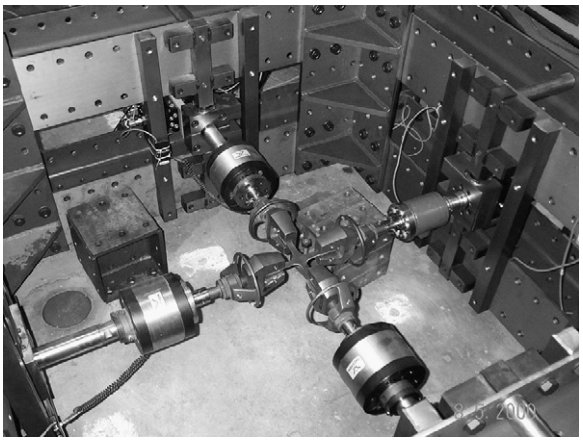

Fig. 1. Plane biaxial test device for cruciform specimens.

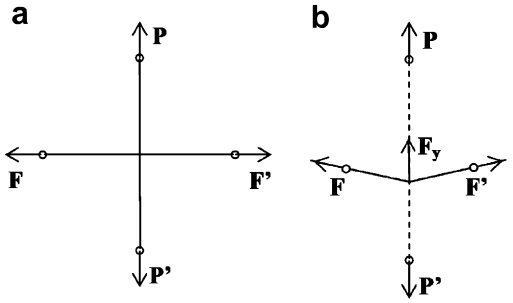

Fig. 2. Forces on the cruciform specimen. (a) Ideal situation; (b) real situation.

shear strains can be quantified and thus eliminate the requirement of a uniform strain field. It is even found out that for the purpose of material parameter identification, strain heterogeneities are necessary since the aim is to create a heterogeneous deformation field and to examine its information content with respect to the four independent orthotropic parameters. In this paper, two geometry types were tested: one completely flat and one with a hole of 8 mm diameter in the centre to increase the strain heterogeneity. The presence of the hole in this study is to influence the overall deformation field and to try to make the measured strain fields more sensitive to the different material parameters, knowing that in a strict theoretical sense this makes no difference. It is clear that the elastic constants of a material do not change when using a different boundary value problem to extract them. However, when dealing with an experimentally obtained strain field, this can be very important. For example, when performing a uniaxial tensile test on a specimen with a very small hole, it will be difficult to measure by DIC the local strain gradients around the hole, which contain crucial information about the shear modulus. In a numerical simulation however, these local strain gradients can be retrieved without any problem.

The hole is realised using a simple vertical drilling machine. It is shown by Fig. 7 that the resulting experimental strain fields are influenced by the presence of the hole. However, possible damage to the fibres and the matrix close to the hole, apparently does not affect the behaviour of the material farther from the hole. Moreover, the information in an area of 2 mm around the hole will not be used in the final identification procedure. The total length of the specimens is 250 mm, the width of the arms 25 mm and the radius of the corner fillet 20 mm (Fig. 3).

The material used is glass fibre reinforced epoxy with a $\left[(+45^\circ \quad -45^\circ \quad 0^\circ)_3(+45^\circ \quad -45^\circ)\right]$-lay-up. This material with this specific lay-up is often used for wind turbine rotor blades as they are globally submitted

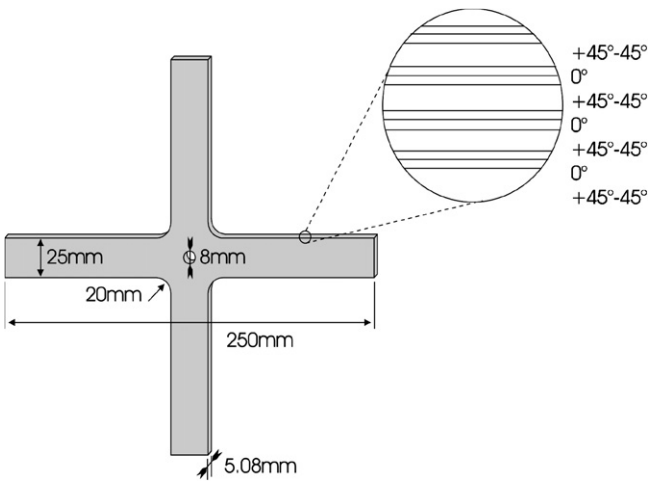

Fig. 3. Cruciform specimen with indication of material lay-up.

to bending combined with torsion, a complex stress state. The (±45°)-layers serve to carry torsion and the (0°)-layers to carry bending. The (±45°)-layers have a thickness of 0.61 mm; the 0°-layers of 0.88 mm resulting in a total nominal thickness of 5.08 mm. The engineering constants E_x, E_y, v_{xy} and G_{xy} that are targeted in this paper are the homogenised values over the thickness (the so-called apparent engineering constants).

2.3. Digital image correlation (DIC)

Displacement and strain determination used on the cruciform specimens is performed by digital image correlation. This technique allows studying qualitatively as well as quantitatively the mechanical behaviour of materials under certain loading conditions and has been used in various technological domains. The DIC technique has been developed in the 1980's and has since then extensively been evaluated (Knauss et al., 2003; Schreier et al., 2000; Sutton et al., 1988) and improved (Bruck et al., 1989; Sutton et al., 1986; Cheng et al., 2002; Yoneyama et al., 2006). However, the fundamental principles of the method remain unchanged and are well described by Peters and Ranson, 1982; Sutton et al., 1983 and Chu et al., 1985.

Each picture taken with a CCD camera corresponds to a different load step. The cameras used in the current set-up use a 1392×1040 pixel gray level 12-bit CCD sensor. Two images of the specimen at different states of deformation are compared by means of a correlation window or an image subset. The image correlation routine allows locating every subset of the initial image in the deformed image by means of a classic correlation function using the sum of the squared differences of the pixel values. The displacement result, expressed in the centre point of the subset, is an average of the displacements of the pixels inside the subset. The step size defines the number of pixels over which the subset is shifted in x- and y-directions to calculate the next result. The size of a subset can be for example 9×9, 11×11, 13×13 pixels etc., the step size can be 1, 2, 3 pixels etc.

For the actual tests a subset size of 19 pixels and a step size of 5 pixels is used. The choice of the correlation window size and the shift or step size is not based on deterministic elements. In the available commercial DIC-systems the subset size is identical throughout the entire image. This means that once the subset size is chosen, it remains identical during the correlation calculation. The size of the subset depends on the type of deformation field to be expected. When dealing with homogeneous deformation (constant displacement gradients), the subset size should be as big as possible to enable noise filtering and thereby smoothing of the displacement data. However, in the case of heterogeneous deformations (variable displacement gradients), the subset size should be a trade-off between smearing out of the displacement data (noise filtering) and correlation problems. When using large subsets, the displacement data is homogenised in an area that does not necessarily correspond to the heterogeneous character of the deformation field. When using small subsets, the grey value pattern is not always unique enough to avoid problems during the correlation calculation. In the present paper a subset size of 19×19 pixels has been chosen to perform the study. This choice is based on experimental experience and moreover it is a fair compromise between the previously cited arguments.

The step size on the other hand only determines the resolution of available displacement data. The smaller the step size, the larger the number of displacement data points and the longer the correlation calculation time. The chosen step size is a compromise between a fair CPU-time and the possibility to treat the displacement data statistically within a given strain window (cfr. next paragraph).

Fig. 4 depicts the sequence of taking a picture of an object before and after loading, storing the images onto a PC trough a frame grabber, performing the correlation of both images – i.e., locating the different undeformed subsets in the deformed image – and finally calculating the corresponding displacement of the centers of the subsets, which finally yields the desired displacement field. The strain field is then calculated by numerical differentiation of the smoothened displacement field as explained in the next paragraph.

2.4. Strain derivation

In this study the experimental and FE-calculated strains are compared as being the responses of the system to the boundary conditions. This means that the experimental strains have to be derived from the measured displacement field. As a step size of 5 pixels is used an experimental displacement value is available every 5 pixels in both horizontal and vertical direction.

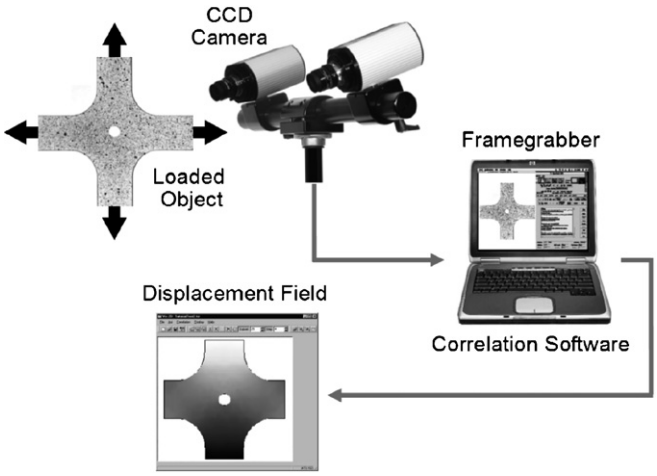

Fig. 4. Working principle of the DIC-system.

The FE-strains are calculated at the Gauss points located in the mesh elements. The objective is to calculate the experimental strains at the same location. A bilinear interpolation function is therefore fitted onto a square region of 5×5 data points (i.e., strain window size) around the coordinates of the Gauss-points in the experimental displacement date field. The choice of a region containing 5×5 data points is based on a trade-off between too much smoothing when using a larger region and a higher noise influence when using a smaller region.

Once the analytical expression of the surface is determined for both the horizontal and the vertical displacement components, it can simply be derived at the considered location in both directions, yielding the different strain components. The resolution of the images in the current set-up is 0.085 mm/pixel. This means that the strain values are based on an area of 1.7×1.7 mm^2. An accuracy of $\pm 10\%$ of the actual strain value can be expected with the current settings. When the elements of the FE-mesh contain only one Gauss point, which is the case in the present study, the strain values are compared in a number of locations equal to the number of elements.

3. Mixed numerical–experimental technique

3.1. Introduction

The mixed numerical–experimental technique used in this paper belongs to the category of inverse problems. In contrast to a direct problem which is the classical problem where a given experiment is simulated in order to obtain the stresses and the strains, inverse problems are concerned with the determination of the unknown state of a mechanical system considered as a black box, using information gathered from the response to stimuli on the system (Bui, 1994). The inverse problem is a problem where certain input data of the direct problem is deduced from the comparison between the experimental results and the numerical FE-simulation of that same problem. Not only the boundary information is used, but relevant information coming from local or full-field surface measurements is also integrated in the evaluation of the behaviour of a given material.

The inverse method described here can actually be narrowed to parameter identification, as the only item of interest to this study is actually the determination of the physically relevant constitutive parameters. The values of the material parameters cannot be derived immediately from the experiment. A numerical analysis is necessary to simulate the actual experiment. However, this requires that the material parameters are known. The identification problem can then be formulated as an optimisation problem where the function to be minimised is some error function that expresses the difference between numerical simulation results and experimental data. In the present case the strains are used as output data. This choice offers two advantages: the

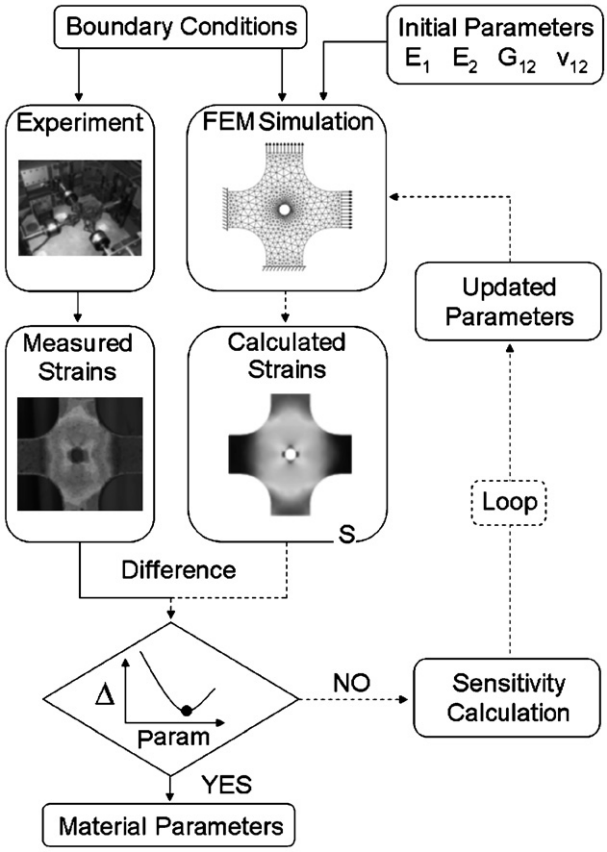

Fig. 5. Flow-chart of the parameter identification problem.

exact knowledge of the boundary conditions is less important and the sensitivity calculation as a part of the optimisation procedure is much faster. Fig. 5 represents the flow-chart of the present inverse modelling problem. The parameters to be identified are the four independent apparent engineering constants E_x, E_y, G_{xy} and v_{xy}. They describe the composite material (matrix and fibres) as a homogeneous entity and they are supposed to be identical for the entire specimen. It is also possible to consider a different set of parameters for every element in the Finite element mesh and to perform the same identification. This last option however, is not treated in the present study.

3.2. Optimisation algorithm and sensitivity calculation

The identification of the four independent apparent engineering constants is based on a Gauss–Newton optimisation method. The cost function that is minimised is expressed in terms of an unweighted least squares formulation. Expression (1) shows the form of cost function $C(\underline{p})$, in which $\underline{p}$ is the vector of material parameters to be identified. The residuals in the function are formed by the differences between the experimental and the numerical strain components ε_x, ε_y and γ_{xy}, expressed numerically as well as experimentally (as explained in Section 2.4) in the Gauss-point of every mesh element. The index "n" in expression (1) stands for the total number of elements in the FE-mesh.

$$C(\underline{p}) = C(\underline{\varepsilon}(\underline{p}), \underline{p}) = \sqrt{\sum_{i=1}^{n} \left(\frac{\varepsilon_{x_i}^{\mathrm{num}}(\underline{p}) - \varepsilon_{x_i}^{\mathrm{exp}}}{\varepsilon_{x_i}^{\mathrm{exp}}} \right)^2 + \left(\frac{\varepsilon_{y_i}^{\mathrm{num}}(\underline{p}) - \varepsilon_{y_i}^{\mathrm{exp}}}{\varepsilon_{y_i}^{\mathrm{exp}}} \right)^2 + \left(\frac{\gamma_{xy_i}^{\mathrm{num}}(\underline{p}) - \gamma_{xy_i}^{\mathrm{exp}}}{\varepsilon_{xy_i}^{\mathrm{exp}}} \right)^2}. \quad (1)$$

The necessary condition for a cost function to attain its minimum is expressed by (2). The partial derivative of the function with respect to the different material parameters has to be zero:

$$\frac{\partial C(\underline{p})}{\partial p_j} = \frac{1}{C(\underline{p})} \sum_{i=1}^{n} \left(\frac{\varepsilon_{x_i}^{\text{num}}(\underline{p}) - \varepsilon_{x_i}^{\text{exp}}}{\varepsilon_{x_i}^{\text{exp}}} \right) \frac{\partial \varepsilon_{x_i}^{\text{num}}}{\partial p_j} + \left(\frac{\varepsilon_{y_i}^{\text{num}}(\underline{p}) - \varepsilon_{y_i}^{\text{exp}}}{\varepsilon_{y_i}^{\text{exp}}} \right) \frac{\partial \varepsilon_{y_i}^{\text{num}}}{\partial p_j} + \left(\frac{\gamma_{xy_i}^{\text{num}}(\underline{p}) - \gamma_{xy_i}^{\text{exp}}}{\varepsilon_{xy_i}^{\text{exp}}} \right) \frac{\partial \varepsilon_{xy_i}^{\text{num}}}{\partial p_j} = 0. \tag{2}$$

Expression (2) has to be written for every single unknown parameter p_j.

As no explicit relationship between the numerical strain components and the different parameters exists, it is not possible to find an analytical solution for the optimal parameter values. The problem has to be solved iteratively by updating the parameter values. Therefore, the different strain components $\varepsilon_x^{\text{num}}$, $\varepsilon_y^{\text{num}}$ and γ_{xy}^{num} are linearised around a given parameter set p^k. This is done by developing a Taylor expansion of the simulated strains around that same parameter set and limiting the expression to the linear terms. The following expression (3) for $\varepsilon_x^{\text{num}}$ is then obtained, in which $(p_j - p_j^k)$ is the difference for a given parameter between the value p_j^k at the working point k and its new estimate p_j.

$$\varepsilon_{x_i}^{\text{num}}(\underline{p}) \cong \varepsilon_{x_i}^{\text{num}}(\underline{p}^k) + \sum_{j=1}^{\text{m}} \left(\frac{\partial \varepsilon_{x_i}^{\text{num}}(\underline{p})}{\partial p_j} \right)_k (p_j - p_j^k) + \Theta^2. \tag{3}$$

The same type of expression can be formulated for $\varepsilon_y^{\text{num}}$ and γ_{xy}^{num}. When substituting these expressions into expression (2) and after rearranging some terms, expression (4) in matrix form, yielding the parameter updates is obtained:

$$\underline{\Delta p} = \left(\underline{\underline{S}}^t \underline{\underline{S}} \right)^{-1} \underline{\underline{S}}^t \left(\underline{\varepsilon}^{\text{exp}} - \underline{\varepsilon}^{\text{num}}(\underline{p}^k) \right), \tag{4}$$

in which the different elements are:

$\underline{\Delta p}$	column vector of the parameter updates for E_x, E_y, G_{xy} and v_{xy}
$\underline{\varepsilon}^{\text{exp}}$	column vector of $\varepsilon_x^{\text{exp}}$, $\varepsilon_y^{\text{exp}}$ and γ_{xy}^{exp} for every mesh element
$\underline{\varepsilon}^{\text{num}}(\underline{p}^k)$	column vector of $\varepsilon_x^{\text{num}}$, $\varepsilon_y^{\text{num}}$ and $\varepsilon_{xy}^{\text{num}}$ as a function of the parameters at iteration k
$\underline{p}^k$	the four apparent engineering constants at iteration step k
$\underline{\underline{S}}$	sensitivity matrix

The sensitivity matrix (expression 5) groups the sensitivity coefficients of the strain components in every element of the FE mesh with respect to the elastic material parameters. This means that the sensitivity matrix contains nothing else than the partial derivatives of the different strain components $\varepsilon_x^{\text{num}}$, $\varepsilon_y^{\text{num}}$ and $\varepsilon_{xy}^{\text{num}}$ with respect to E_x, E_y, G_{xy} and v_{xy}, for every element of the mesh.

$$\underline{\underline{S}} = \begin{bmatrix} \frac{\partial \varepsilon_x^1}{\partial E_x} & \frac{\partial \varepsilon_x^1}{\partial E_y} & \frac{\partial \varepsilon_x^1}{\partial G_{xy}} & \frac{\partial \varepsilon_x^1}{\partial v_{xy}} \\ \frac{\partial \varepsilon_y^1}{\partial E_x} & \frac{\partial \varepsilon_y^1}{\partial E_y} & \frac{\partial \varepsilon_y^1}{\partial G_{xy}} & \frac{\partial \varepsilon_y^1}{\partial v_{xy}} \\ \frac{\partial \gamma_{xy}^1}{\partial E_x} & \frac{\partial \gamma_{xy}^1}{\partial E_y} & \frac{\partial \gamma_{xy}^1}{\partial G_{xy}} & \frac{\partial \gamma_{xy}^1}{\partial v_{xy}} \\ \vdots & \vdots & \vdots & \vdots \\ \frac{\partial \varepsilon_x^n}{\partial E_x} & \frac{\partial \varepsilon_x^n}{\partial E_y} & \frac{\partial \varepsilon_x^n}{\partial G_{xy}} & \frac{\partial \varepsilon_x^n}{\partial v_{xy}} \\ \frac{\partial \varepsilon_y^n}{\partial E_x} & \frac{\partial \varepsilon_y^n}{\partial E_y} & \frac{\partial \varepsilon_y^n}{\partial G_{xy}} & \frac{\partial \varepsilon_y^n}{\partial v_{xy}} \\ \frac{\partial \gamma_{xy}^n}{\partial E_x} & \frac{\partial \gamma_{xy}^n}{\partial E_y} & \frac{\partial \gamma_{xy}^n}{\partial G_{xy}} & \frac{\partial \gamma_{xy}^n}{\partial v_{xy}} \end{bmatrix} \quad \text{sensitivity matrix} \tag{5}$$

Table 1
Derivatives of the strain components with respect to the four independent parameters

	E_x	E_y	v_{xy}	G_{xy}
$\frac{\partial \varepsilon_x^{num}}{\partial p}$	$-\frac{\sigma_x}{E_x^2}+\frac{v_{xy}}{E_x^2}\sigma_y$	$\frac{v_{xy}}{E_x E_y}\sigma_y$	$-\frac{\sigma_y}{E_x}$	0
$\frac{\partial \varepsilon_y^{num}}{\partial p}$	$\frac{v_{xy}}{E_x^2}\sigma_x$	$\frac{v_{xy}}{E_x E_y}\sigma_x-\frac{\sigma_y}{E_y^2}$	$-\frac{\sigma_x}{E_x}$	0
$\frac{\partial \gamma_{xy}^{num}}{\partial p}$	0	0	0	$-\frac{\sigma_{xy}}{G_{xy}^2}$

The components of this sensitivity matrix can be derived analytically from the constitutive relation between stress and strain, which is given by expression (6) in the case of a plane stress problem.

$$\begin{Bmatrix} \varepsilon_x^{num} \\ \varepsilon_x^{num} \\ \gamma_{xy}^{num} \end{Bmatrix} = \begin{bmatrix} \frac{1}{E_x} & -\frac{v_{yx}}{E_y} & 0 \\ -\frac{v_{xy}}{E_x} & \frac{1}{E_y} & 0 \\ 0 & 0 & \frac{1}{G_{xy}} \end{bmatrix} \begin{Bmatrix} \sigma_x \\ \sigma_y \\ \tau_{xy} \end{Bmatrix} \tag{6}$$

Due to the symmetry of the matrix containing the material parameters, v_{yx} can be expressed as a function of v_{yx}, E_x and E_y (7):

$$\frac{v_{xy}}{E_x}=\frac{v_{yx}}{E_y}. \tag{7}$$

The twelve elements of the sensitivity matrix belonging to one and the same element in the FE mesh are expressed in Table 1.

The values of the different stress components and the different parameters appearing in the expression of the derivatives in Table 1 are taken from the current iteration step. This means that for the first iteration the sensitivity coefficients are calculated with the starting values of the different parameters and with the stress components obtained by the first simulation. The criterion used to end the iteration process is based on the relative values of the parameter updates. Once they are below the limit of 0.5% of the current parameter value, the identification routine is stopped.

4. Experimental results

4.1. Traditional tests on beamlike specimens

An extended database of experimental static and fatigue results on beamlike glass fibre reinforced epoxy specimens with a $\left[(+45^\circ \quad -45^\circ \quad 0^\circ)_3(+45^\circ \quad -45^\circ)\right]$-lay-up has been set-up within the framework of a project that deals with the optimisation of the use of composite materials for wind turbine rotor blades. One of the aims of the project is to investigate the material behaviour under complex stress states. For the glass fibre reinforced composite laminate with the mentioned lay-up the average and standard deviation material parameter results of about 400 traditional beamlike tests are given in Table 2. No information about the

Table 2
Material properties of the laminate obtained on beamlike specimens

	E_x (GPa)	E_y (GPa)	v_{xy}
Average	27.03	14.21	0.455
Standard deviation	1.19	0.85	0.042

Table 3
Material properties of the ply used in the laminate obtained on beamlike specimens

	E_1 (GPa)	E_2 (GPa)	G_{12} (GPa)	v_{12}
Average	39.10	14.44	5.39	0.294
Standard deviation	2.10	0.98	1.77	0.027

Table 4
Calculated material properties of the laminate using classical laminate theory

	E_x (GPa)	E_y (GPa)	G_{xy} (GPa)	v_{xy}
Average	28.48	16.27	8.33	0.407

The apparent engineering constants of the laminate.

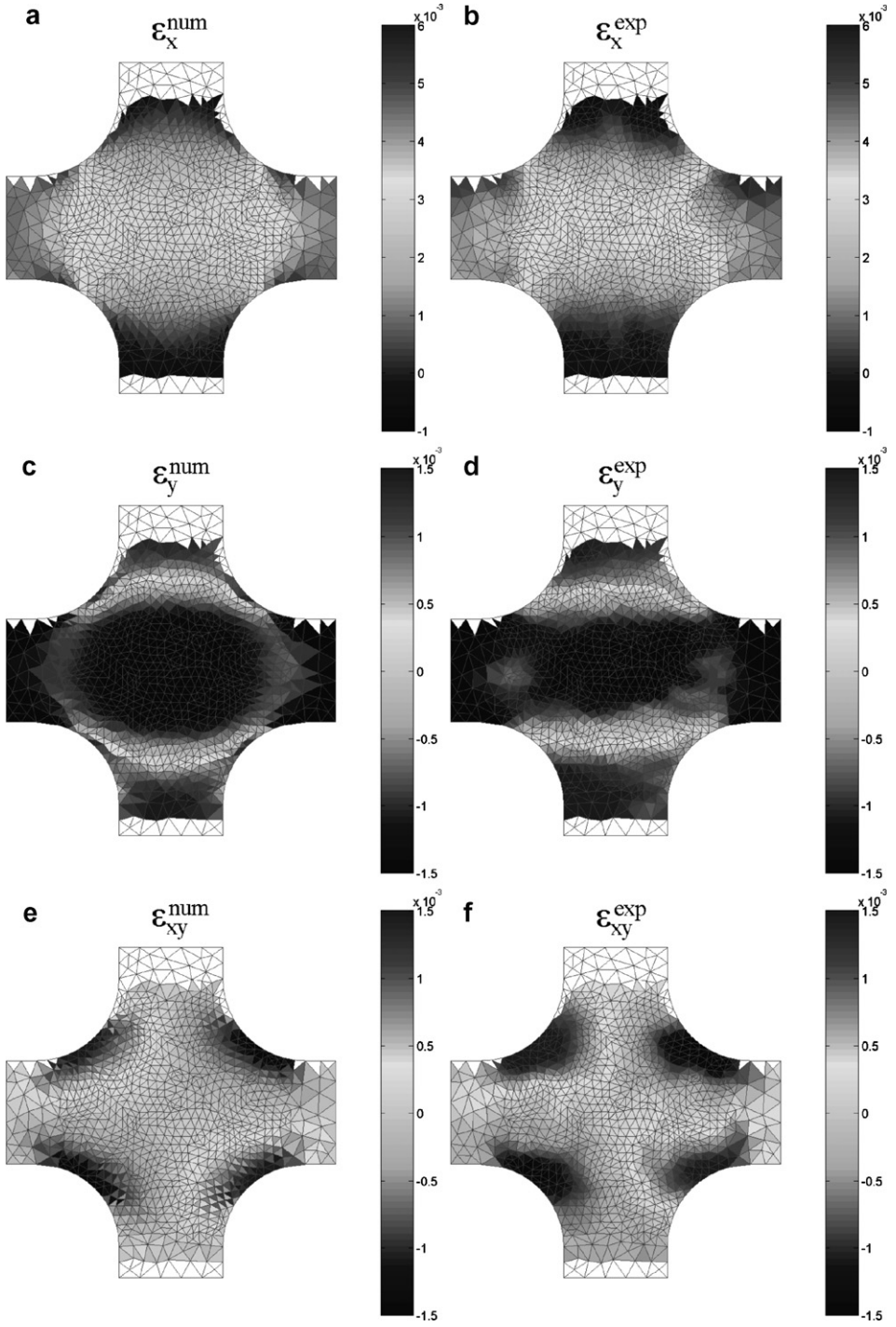

Fig. 6. FEM strains (a), (c), (e) and experimental strains (b), (d) and (f) for non-perforated specimen.

shear modulus is available for this lay-up. Only for a single lamina, information exists from off-axis tests and tests on a (+45°/−45°) lay-up (Table 3). Based on the ply data, the theoretically expected properties of the laminate can be calculated using classical laminate theory (Table 4).

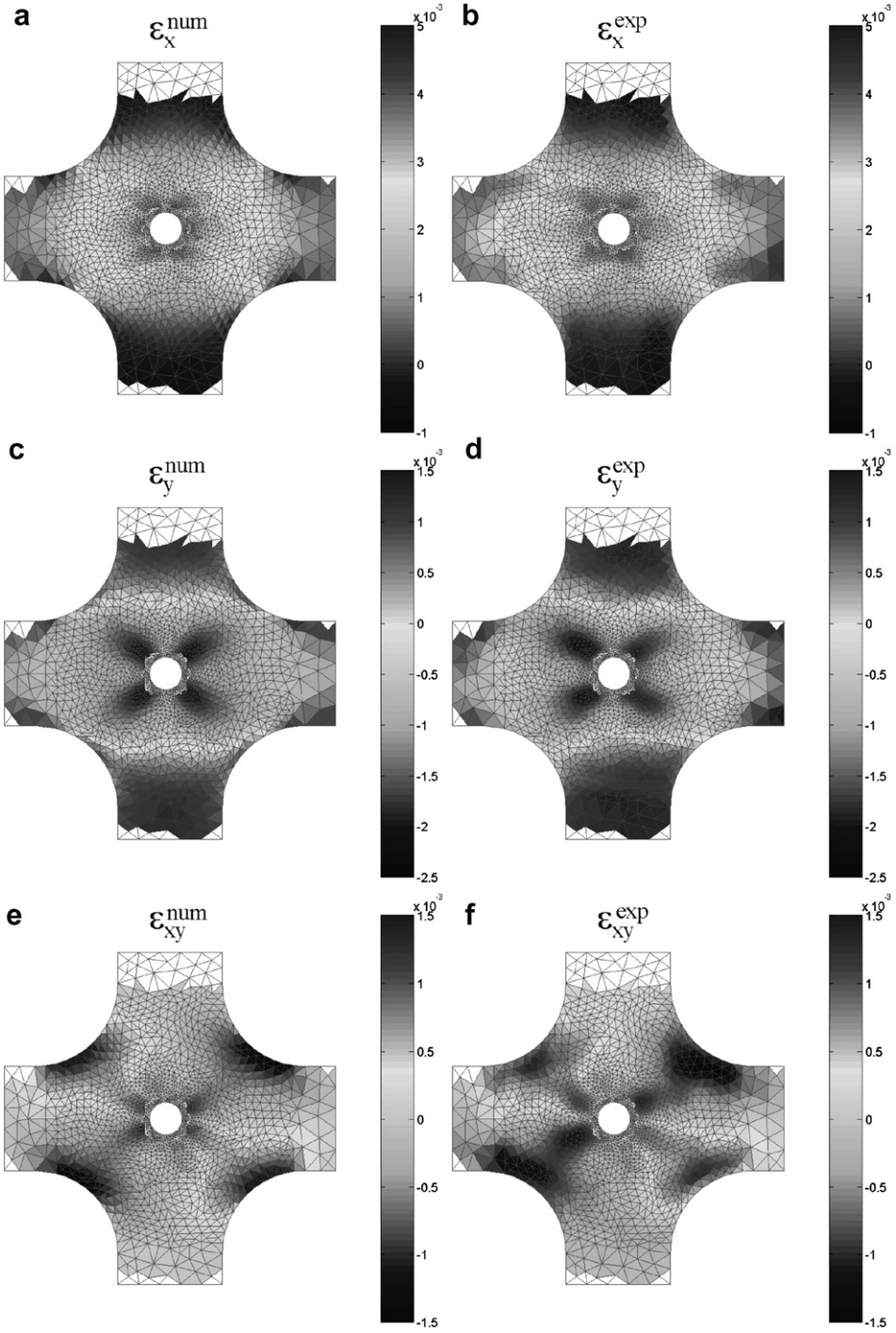

Fig. 7. FEM strains (a), (c), (e) and experimental strains (b), (d) and (f) for perforated specimen.

4.2. Results of mixed numerical–experimental technique

For the identification of the four independent elastic orthotropic parameters, two test specimens are used; a perforated and a non-perforated specimen. Three different ratios between the horizontal (X-direction) and the vertical (Y-direction) tensile load are used during deformation of the specimens; 2.56/1, 3.85/1 and 5.77/1. Five successive load steps are imposed per ratio. This means that fifteen independently measured strain field triplets (ε_x, ε_y and γ_{xy}) are available per specimen for the identification process. The same loads are used in the FEM-simulation. A plane stress model is used with a uniformly distributed load as boundary condition. This is a hypothesis that is verified when looking at the strain plots in Figs. 6 and 7. The figures clearly show that the strain field exposes a fairly symmetrical pattern, which means that the actual load is uniformly distributed. In the case of the perforated specimen, a circular region around the hole with a width of 2 mm is considered from which no experimental data is used. Due to the steep gradients in the displacement field close to the hole it is difficult to obtain reliable strain values. Therefore these values are not used in the identification procedure.

The convergence criterion used in the optimisation phase ends the iteration process when the relative value of the parameter updates is inferior to 0.5%. In all of the optimisation runs, the convergence criterion is reached in less than 13 iterations. The results of the identification process are shown in Tables 5 and 6 for both perforated and non-perforated specimen, in terms of the mean parameter value and its corresponding standard deviation. They are obtained based on the 15 imposed load steps considered per specimen. The starting values for each of the parameters are mentioned as well.

It can be observed that the difference between the results for both specimen types is reasonably small. The stability of the results obtained with the non-perforated specimen is slightly larger. This is probably due to the fact that the strain field is less complex and therefore easier to measure than in the case of the perforated specimen. Figs. 6 and 7 show the different strain fields for both specimen types. The plots for the different simulated strain fields at a given load step are obtained using the mean identified material parameters presented in Tables 5 and 6.

The scaling is the same for both experimental and numerical strains and the experimental values are represented in the FEM-mesh. The colour of the plots is chosen in such a way that the similarity between both types of deformation fields is clearly visible and the results are not smoothened. The mesh triangles, in which no colour value is shown, correspond to the regions of the cruciform specimen in which the experimental results are not available (in the vicinity of the hole and in a part of the arms of the specimen).

The plots are showing a significant agreement between the measured and the simulated results. It is clear however, that the real behaviour of the specimens is not completely symmetrical. The reason therefore is that the loading conditions are probably not ideally symmetrical or that the composite specimen itself is not com-

Table 5
Material properties obtained on perforated cruciform specimen

	E_x (GPa)	E_y (GPa)	G_{xy} (GPa)	v_{xy}
Starting values	15	10	10	0.3
Average	23.73	12.91	8.61	0.455
Standard deviation	0.88	1.05	0.46	0.042

The apparent engineering constants of the laminate.

Table 6
Material properties obtained on non-perforated cruciform specimen

	E_x (GPa)	E_y (GPa)	G_{xy} (GPa)	v_{xy}
Starting values	15	10	10	0.3
Average	24.90	13.07	9.19	0.475
Standard deviation	0.46	0.65	0.54	0.030

The apparent engineering constants of the laminate.

pletely homogeneous. Therefore the identified parameters are a characterisation of the mean or homogenised behaviour of the material under the given loading conditions.

5. Conclusions

An inverse method has been proposed to determine the apparent engineering constants (E_x, E_y, G_{xy} and v_{xy}) of a glass fibre reinforced epoxy with a $\left[(+45^\circ \quad -45^\circ \quad 0^\circ)_3(+45^\circ \quad -45^\circ)\right]$-lay-up. Two specimen geometries are used: a regular cruciform specimen and a cruciform specimen into which a central hole is drilled. The latter one is made in order to enhance the already heterogeneous deformation field. The method is based on a finite element calculated strain field of a cruciform specimen loaded in both orthogonal axes and the measured strain field obtained by digital image correlation. A least-squares formulation of the difference between the experimental and the numerical strains is used along with a Gauss–Newton optimisation algorithm. The obtained material parameters are very well in agreement with the values obtained by traditional uniaxial tensile tests. However, the results based on the regular specimen show less variance than the results obtained with the perforated specimen. This is possibly due to the fact that the DIC-technique has some difficulties measuring steep deformation gradients, hence inducing errors in the measurement of the displacement and strain maps. The objective of the experiment is to enforce a material behaviour that exposes the different elastic material parameters. If this is achieved by a non-perforated specimen, there is no need for a more complex geometry possibly leading to more measurement errors.

Acknowledgements

This project is supported by the Belgian Science Policy through the IAP P05/08 project and the European Commission in the framework of the specific research and technology development programme Energy, Environment and Sustainable Development with contract number ENK6-CT-2001-00552. The authors also express their gratitude to Hans Tommerup Knudsen from LM-Glassfiber in Denmark for his effort in producing the cruciform specimens.

References

Amiot, F., Hild, F., Roger, J.P., 2005. Model and parameter identification using non-contact loading and full-field measurement. In: Proceedings of the SEM Conference on Experimental and Applied Mechanics, Oregon, USA.

ASTM, 2000. D3039-00 Standard test method for tensile properties of polymer matrix composite materials. In: Annual book of ASTM standards, vol. 15, no. 03.

ASTM, 2001. D4255-01 Standard test method for in-plane shear properties of polymer matrix composite materials by the rail shear method. In: Annual book of ASTM standards, vol. 15, no. 03.

Bruck, H.A., McNeil, S.R., Sutton, M.A., Peters, W.H., 1989. Digital image correlation using Newton–Raphson method of partial differential correction. Experimental Mechanics 29 (3), 261–267.

Bruno, L., Poggialini, A., 2005. Elastic characterization of anisotropic materials by speckle interferometry. Experimental Mechanics 45 (3), 205–212.

Bui, H.D., 1994. Inverse Problems in the Mechanics of Materials: An Introduction. CRC Press Inc., Florida.

Cárdenas-García, J.F., 2000. Determination of the elastic constants using Moiré. Mechanics Research Communications 27 (1), 69–77.

Cárdenas-García, J.F., Ekwaro-Osire, S., Berg, J.M., Wilson, W.H., 2005. Non-linear least-squares solution to the Moiré hole method problem in orthotropic materials. Part II: Material elastic constants. Experimental Mechanics 45 (4), 314–324.

Chaudonneret, M., Gilles, P., Labourdette, R., Policella, H., 1997. Machine d'essais de traction biaxiale pour essais statiques et dynamiques. La Recherche Aérospatiale 5, 299–305.

Cheng, P. et al., 2002. Full-field speckle pattern image correlation with B-spline deformation function. Experimental Mechanics 42, 344–352.

Chu, T.C., Ranson, W.F., Sutton, M.A., Peters, W.W., 1985. Applications of digital image correlation techniques to experimental mechanics. Experimental Mechanics 25 (3), 232–244.

Dawicke, D.S., Pollock, W.D., 2000. Biaxial testing of 2219-T87 aluminum alloy using cruciform specimens. Nasa Contractor Report 4782, pp. 1–46.

Ellyn, F., Wolodko, J.D., 1995. Testing facilities for multiaxial loading of tubular specimens. In: Proceedings of the 1995 Symposium on multiaxial fatigue and deformation testing techniques. SAE Denver, pp. 7–24.

Ferron, G., Makinde, A., 1988. Design and development of a biaxial strength testing device. Journal of Testing and Evaluation 16 (3), 253–256.

Furgiuele, F.M., Muzzupappa, M., Pagnotta, L., 1997. A full-field procedure for evaluating the elastic properties of advanced ceramics. Experimental Mechanics 37, 285–291.

Genovese, K., Lamberti, L., Pappalettere, C., 2004. A new hybrid technique for in-plane characterization of orthotropic materials. Experimental Mechanics 44 (6), 584–592.

Grédiac, M., 2004. The use of full-field measurement methods in composite material characterization: interest and limitations. Composites: Part A 35, 751–761.

Grédiac, M., Pierron, F., Surrel, Y., 1999. Novel procedure for complete in-plane composite characterization using a single T-shaped specimen. Experimental Mechanics 39, 142–149.

Grédiac, M., Toussaint, E., Pierron, F., 2002. Special virtual fields for the direct determination of material parameters with the virtual fields method: Application to in-plane properties. International Journal of Solids and Structures 39, 2707–2730.

Huang, L., Sun, X., Liu, Y., Cen, Z., 2004. Parameter identification for two-dimensional orthotropic material bodies by the boundary element method. Engineering Analysis with Boundary Elements 28, 209–221.

Knauss, W.G., Chasiotis, I., Huang, Y., 2003. Mechanical measurements at the micron and nanometer scales. Mechanics of Materials 35, 217–231.

Lefebvre, D., Chebl, C., Thibodeau, L., Khazzari, E., 2000. A high-strain biaxial testing rig for thin-walled tubes under axial load and pressure. Experimental Mechanics 40 (3), 312–320.

Le Magorou, L., Bos, F., Rouger, F., 2002. Identification of constitutive laws for wood-based panels by means of an inverse method. Composites Science and Technology 62, 591–596.

Makinde, A., Thibodeau, L., Neale, K.W., 1992. Development of an apparatus for biaxial testing using cruciform specimens. Experimental Mechanics 32 (2), 138–144.

Mayes, J.S., Welsh, J.S., Key, C.T., 2002. Biaxial failure envelope for a glass fabric reinforced composite laminate. In: Final Report PO N00167-01-M-0246, Mayes Consulting Engineers, pp. 1–13.

Meuwissen, M., 1998. An Inverse Method for the Mechanical Characterization of Metals. Ph.D. Thesis, Eindhoven University of Technology, The Netherlands.

Meuwissen, M.H.H., Oomens, C.W.J., Baaijens, F.P.T., Petterson, R., Janssen, J.D., 1998. Determination of the elasto-plastic properties of aluminium using a mixed numerical–experimental method. Journal of Materials Processing Technology 75, 204–211.

Molomard, J., Le Riche, R., Vautrin, A., Lee, J.R., 2005. Identification of the four orthotropic plate stiffnesses using a single open-hole tensile test. Experimental Mechanics 45 (5), 404–411.

Peters, W.H., Ranson, W.F., 1982. Digital imaging techniques on experimental stress analysis. Optical Engineering 21 (3), 427–431.

Schreier, H.W., Braasch, J.R., Sutton, M.A., 2000. Systematic errors in digital image correlation caused by intensity interpolation. Optical Engineering 39 (11), 2915–2921.

Shiratori, E., Ikegami, K., 1967. A new biaxial tensile testing machine with flat specimen. In: Bulletin of Tokyo Institute of Technologie 82, pp. 105–118.

Sutton, M.A., Wolters, W.J., Peters, W.H., Ranson, W.F., McNeil, S.R., 1983. Determination of displacements using an improved digital correlation method. Image Vision Computing 1 (3), 133–139.

Sutton, M.A., Cheng, M., Peters, W.H., Chao, Y.J., McNeil, S.R., 1986. Application of an optimized digital image correlation method to planar deformation analysis. Image Vision Computing 4 (3), 143–150.

Sutton, M.A., McNeil, S.R., Jang, J., Babai, M., 1988. The effect of subpixel image resaturation on digital image correlation estimates. Optical Engineering 27 (10), 870–877.

Szostkiewicz, C., Mailler, P., Hamelin, P., 1997. Mixed numerical and experimental stiffness identification methods for soft textile composites. In: Proceedings of the Euromech Colloquium, Kerkrade, The Netherlands.

Wang, W.T., Kam, T.Y., 2000. Material characterization of laminated composite plates via static testing. Composite Structures 50, 347–352.

Wang, Z., Cardénas-Garcia, J.F., Han, B., 2005. Inverse method to determine elastic constants using a circular disk and Moiré interferometry. Experimental Mechanics 45 (1), 27–34.

Whitney, J.M., Daniel, I.M., Byron Pipes, R., 1984. In: Experimental Mechanics of Fiber Reinforced Composite Materials. The Society for Experimental Mechanics. Prentice-Hall Inc.

Yoneyama, S., Kikuta, H., Kitagawa, A., Kitamura, K., 2006. Lens distortion correction for digital image correlation by measuring rigid body displacement. Optical Engineering 45 (2), 023602.

Yu, Y., Wan, M., Wu, X.D., Zhou, X.B., 2002. Design of a cruciform biaxial tensile specimen for limit strain analysis by FEM. Journal of Materials Processing Technology 123 (1), 67–70.

Zhu, J., 1996. Measurement of Poisson's ratio of non-metallic materials by laser holographic interferometry. In: Proceedings of the 14th WCNDT, New Delhi, India, pp. 1481–1484.

Zouani, A., Bui-Quoc, T., Bernard, M., 1996. A proposed device for biaxial tensile fatigue testing. Fatigue and Fracture, ASME PVP-323, vol. 1, pp. 331–339.